CHEMISTRY
A EUROPEAN JOURNAL

DOI: 10.1002/chem.200501241

Photoelectrochemical Kinetics of Eosin Y-Sensitized Zinc Oxide Films Investigated by Scanning Electrochemical Microscopy

Yan Shen,[a, b] Kazuteru Nonomura,[c] Derck Schlettwein,[c] Chuan Zhao,[a] and Gunther Wittstock*[a]

Abstract: Eosin Y is used as a sensitizer for nanoporous zinc oxide films for prospective applications in photoelectrochemical solar cells. The kinetics of the reduction of the intermittently formed photo-oxidized dye molecules by iodide ions in the electrolyte phase was investigated by using the feedback mode of scanning electrochemical microscopy (SECM). The bulk solution phase contained triiodide as electron transfer mediator, from which the ultramicroelectrode-generated iodide ions acted as electron donors for photo-oxidized Eosin Y molecules (D^+_{ads}) at the zinc oxide sample. Effective rate constants for the dye regeneration could be extracted from the SECM approach curves. The effective rate constants at different triiodide concentrations could be related to the rate constant for the reaction of the dissolved donor with photo-oxidized Eosin Y bound to ZnO, as well as to the overall rate of the photosensitization process. For the reaction $D^+_{ads} + 1.5\,I^- \rightarrow D_{ads} + 0.5\,I_3^-$ a rate constant of $k_{ox} = (1.4 \pm 0.8) \times 10^8\ cm^{9/2} mol^{-3/2} s^{-1}$ was determined.

Keywords: kinetics · scanning electrochemical microscopy · sensitizers · solar cells · zinc oxide

Introduction

The requirement to develop inexpensive renewable energy sources has stimulated new approaches for the preparation of efficient, low-cost photovoltaic cells. Dye-sensitized solar cells (DSSC) constitute one of the main targets in this direction, since O'Regan and Grätzel[1] have demonstrated that a combination of a nanocrystalline wide-bandgap semiconductor, an adsorbed dye with an absorption band in the visible region, and an appropriate electrolyte system could lead to remarkable conversion efficiencies while avoiding photocorrosion of the semiconductor material. The function of DSSC is based upon electron injection from a photoexcited state of the dye into the conduction band of a wide-bandgap semiconductor. The resulting dye cation is then re-reduced by redox species in the electrolyte.[2] To achieve a high photocurrent quantum yield, this re-reduction of the dye cation must be much faster than the charge recombination reaction between the oxidized dye and injected electrons in the semiconductor or oxidized electrolyte components. Furthermore, a fast re-reduction is also necessary to avoid photodecomposition of the dye.

While initial work was mainly performed on nanocrystalline titania in the anatase form and ruthenium coordination complexes as sensitizers, the present experiments also include a range of other semiconducting metal oxides.[3] To improve the power conversion efficiency further, many authors have focused on design of more efficient sensitizers[4,5] and control of the morphology of the nanostructured semiconductor film.[6,7] There is particular appeal in semiconductor systems that can be processed to functional films with very few processing steps or on a variety of substrates, preferably low-cost, light, mechanically flexible polymers. The samples described in this paper follow such an approach: zinc oxide is deposited electrochemically on a transparent electrode from an aqueous electrolyte in the presence of the dye Eosin Y, which is not only an efficient sensitizer; it also

[a] Dr. Y. Shen, Dr. C. Zhao, Prof. Dr. G. Wittstock
Institut für Reine und Angewandte Chemie und
Institut für Chemie und Biologie des Meeres
Fakultät für Mathematik und Naturwissenschaften
Carl-von-Ossietzky University Oldenburg
26111 Oldenburg (Germany)
Fax (+49) 441-798-3979
E-mail: gunther.wittstock@uni-oldenburg.de

[b] Dr. Y. Shen
Hanse-Wissenschaftskolleg, Lehmkuhlenbusch 4
27753 Delmenhorst (Germany)

[c] K. Nonomura, Prof. Dr. D. Schlettwein
Institut für Angewandte Physik, Justus-Liebig-University Gießen
Heinrich Buff-Ring 16, 35392 Gießen (Germany)

Supporting information for this article is available on the WWW under http://www.chemeurj.org/ or from the author.

acts as a structure-directing agent (SDA) to shape the morphology of the nanocrystalline ZnO deposited.[8] Highly porous yet crystalline sensitized ZnO is obtained in one step and at temperatures below 70 °C. Recently, it was discovered that the dye loading could be increased substantially when ZnO was deposited in the presence of the SDA Eosin Y. The efficiency of the electrodes could be increased further if Eosin Y was then extracted with dilute KOH solution, and Eosin Y or another dye as a sensitizer was finally re-adsorbed from solution onto the nanoporous ZnO.[9]

Despite the substantial accumulation of knowledge about structure–function relationships concerning dyes, semiconductors, and their interactions, relatively little is known about the factors that control the regeneration of the dye molecules after electron injection from the photoexcited dye into the semiconductor conduction band by electron transfer (ET) from dissolved electron donors.[10] This interfacial kinetic process is clearly crucial to the operation of a photoelectrochemical cell, because it is a necessary elementary step when a photocurrent is produced. Fast kinetics of this regeneration step can suppress competing decomposition reactions and the back-transfer of electrons from the semiconductor, a major recombination route and hence a loss mechanism in DSSC. The lack of detailed data for this interfacial regeneration process is partly due to the experimental difficulties encountered in such measurements by conventional electrochemical techniques.

Scanning electrochemical microscopy (SECM) has been demonstrated to be an effective technique for determining ET kinetics at various interfaces, including polymer/liquid[11] and liquid/liquid ones,[12–15] and redox enzymes[16,17] on solid supports. Even immobilized non-redox enzymes[18] can be investigated. Electron transfer reactions at semiconductor/electrolyte interfaces have been studied from various perspectives. Precursor sites on passivated valve metals (TiO_2, Ta_2O_5, Al_2O_3) were identified as locations at which ET reactions occur to form dissolved species in the dark before the onset of pitting corrosion.[19–23] The kinetics of hole injection into GaAs by a probe-generated oxidizer in the dark was studied and applied to local semiconductor etching.[24] SECM feedback investigations at WSe_2 and Si immersed in an electrolyte showed a correlation between the heterogeneous redox kinetics at the sample and the concentration of the majority carriers in it.[25] Photoelectrochemical reactions at semiconductor surfaces have been studied at TiO_2 photocatalysts.[26] The behavior of a TiO_2 (microcrystalline anatase) was compared with the characteristics of bare indium tin oxide (ITO). When probed with the $[Fe(CN)_6]^{4-/3-}$ redox couple, the surface behaved like an insulator in the dark and like a conducting surface under UV illumination. Unwin et al.[27,28] studied the kinetics of photoelectrochemical decomposition of 4-chlorophenol at a TiO_2 particle film under UV illumination using a transient SECM working mode. Haram and Bard[29] determined apparent pseudo-first-order rate constants from steady-state SECM feedback approach curves for the reduction of methyl viologen (MV^{2+}) to the methyl viologen radical cation (MV^{+}) at CdS thin films obtained from wet chemical deposition, as well as their dependence on light intensity and on the concentration of redox species in the electrolyte. In their study the holes in CdS particles were scavenged by dissolved triethanolamine.

In this work we have studied the charge transfer kinetics between I^- and photo-oxidized dye molecules (Eosin Y^+) adsorbed on a wide-bandgap semiconductor (ZnO) during illumination with visible light. We used a complex dye-sensitized electrode such as is currently under investigation for DSSCs. To make the measurements, it was necessary to select a model electrolyte that deviated from the composition of a typical I^-/I_3^- electrolyte system in DSSC applications. A pseudo-first-order rate constant for the reaction of I^- with the sensitized nanoporous film was obtained from steady-state feedback measurements by a procedure inspired by reference [30] in which the electron transfer kinetics was studied at ferrocene-terminated self-assembled monolayers.

Results and Discussion

SECM feedback mode investigation of Eosin Y-sensitized ZnO film: The main difficulty in the SECM feedback investigation was the selection and optimization of the mediator solution. It should contain only one redox form of the mediator couple and should not undergo homogeneous photochemical reactions. In theory, many possible ways of matching dyes and semiconductors with an electrolyte system exist. One of the most commonly used electrolyte systems is I^-/I_3^-. Iodide (I^-) shows favorable energetics and kinetics for the regeneration of the sensitizer molecules, whereas triiodide (I_3^-) displays unusually slow kinetics for the reduction by electrons from the conduction band of the semiconductor interface, but fast kinetics for the reduction at the platinum counter-electrode of a DSSC.

To generate a flux of I^- at the ultramicroelectrode (UME), we used a solution formed by mixing equimolar amounts of I_2 and KI solutions in acetonitrile with tetrabutylammonium trifluoromethanesulfonate (TBAS) as an inert supporting electrolyte. Since the equilibrium constant for the reaction $I^- + I_2 \rightarrow I_3^-$ is $10^7\,L\,mol^{-1}$[31] in acetonitrile, the concentration of I^- and I_2 is only 1% of the concentration of I_3^- for a solution that contains a total of $1\,mol\,cm^{-3}$ KI_3

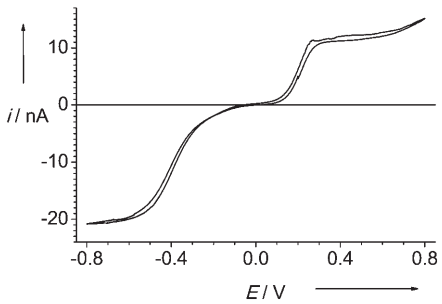

Figure 1. Cyclic voltammogram of 1.1 mM I_3^- + 0.1 M TBAS in acetonitrile solution at a Pt UME, scan rate $0.05\,V\,s^{-1}$.

(1 mM). Figure 1 shows the cyclic voltammogram of such a solution at a Pt microdisk electrode in the bulk phase of the solution. It shows a well-defined reduction wave for reaction (1) and an oxidation wave for the reaction $I_3^- \rightarrow 1.5\,I_2 + e^-$.

$$I_3^- + 2\,e^- \rightarrow 3\,I^- \quad (1)$$

If an equimolar mixture of KI and I_2 is indeed obtained, there is a region around 0 V (versus the Pt pseudo-reference electrode) where no current flows. SECM experiments were carried out at a UME potential $E_T = -0.7$ V where a diffusion-controlled reduction of I_3^- took place and I^- was produced. The approach curves to glass and their excellent agreement with the theory for hindered diffusion indicate that this reaction system can be treated with reasonable accuracy by using the theory developed for a simple redox couple (see below). In the following treatment we assume, as a simplification, that the bulk phase of the solution contains only I_3^- but no I_2 or I^-.

Figure 2 illustrates the principle of the SECM feedback mode in a DSSC system under short-circuit conditions: in feedback mode, I^- is generated by an electrochemical reaction at the UME and diffuses to the dye-sensitized electrode. When the substrate (ZnO/Eosin Y film) is illuminated from the back, I^- can transmit an electron to Eosin Y^+ (Y^+) molecules. In this process the mediator is oxidized back to its original oxidation state, I_3^- [Eq. (2)].

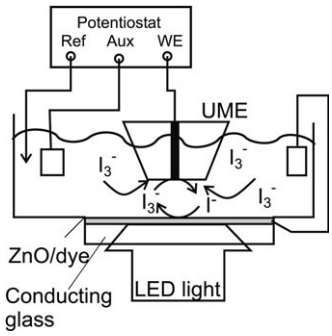

Figure 2. Basic arrangement for probing the heterogeneous reaction at the dye-sensitized semiconductor surface (gray) in the feedback mode under short-circuit conditions. The mediator is triiodide. The broad, hollow arrow indicates the back illumination.

$$1.5\,I^- + Y^+ \rightarrow 0.5\,I_3^- + Y \quad (2)$$

After diffusion to the UME, I_3^- can be reduced again. The experiment gives current variations at the UME as a function of UME–sample distance d and rate of I_3^- regeneration at the sample. From the mathematical description of the mass transport and interfacial kinetics at the sample, a pseudo-first-order rate constant k_{eff} for the reaction at the sample can be extracted.[12]

To verify the suitability of the mediator solution and the absence of any significant photoelectrochemical effects at the Pt UME probe, approach curves were recorded above glass substrates without a ZnO/Eosin Y film in the dark and under illumination (Figure 3). The curves are presented in normalized coordinates $I_T(L)$ versus L, where the normalized current at the UME $I_T = i_T/i_{T,\infty}$ with i_T = the current at the UME and $i_{T,\infty}$ = the current in the bulk solution. The normalized distance L is the distance d in units of the UME radius r_T. The curves agree within experimental error with the theoretical approach curve to an insulating and inert sample expected for a UME of this geometry. This curve, denoted by $I_{T,ins}(L)$, represents the effect of hindered diffusion only, because no reaction occurs at the glass surface. The perfect agreement of the experimental curves with the theory of hindered diffusion supports the general applicability of this mediator system. Corresponding experiments were subsequently carried out at the ZnO/Eosin Y films. In the dark the response $I_{T,ins}(L)$ is equal to that of glass (Figure 4, curve 1) for any mediator concentration, confirming the absence of any electrochemical reaction of I^- with the modified film in the dark. When the film was back-illuminated, the current was significantly larger than in the dark (Figure 4, curves 2–7). The exact curve $I_T(L)$ can be described by Equation (3) for a first-order reaction at the sample and infinitely fast reaction at the UME[12]

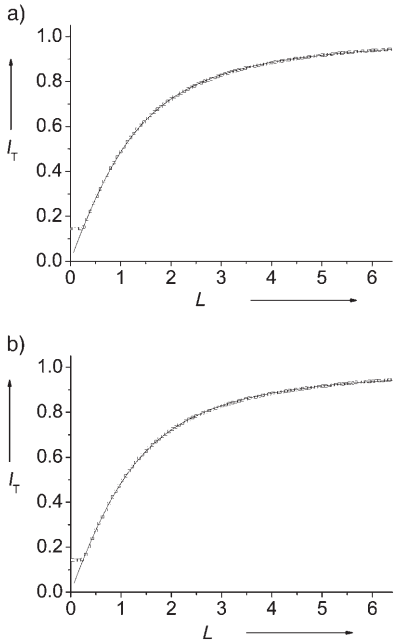

Figure 3. Normalized SECM feedback approach curves in 1.97 mM I_3^- for the approach of a Pt disk electrode, $r_T = 15.0$ μm, toward glass: a) in the dark; b) under illumination by a blue LED. Open symbols are experimental points; the solid line is based on theoretical results, calculated according to reference [33] for an insulator and with RG = 10.2. Scan rate = 1 μm s^{-1}, $E_T = -0.7$ V. The glass sheath of the UME touched the sample at $L = 0.2$. Points at $L < 0.2$ deviate from the theory.

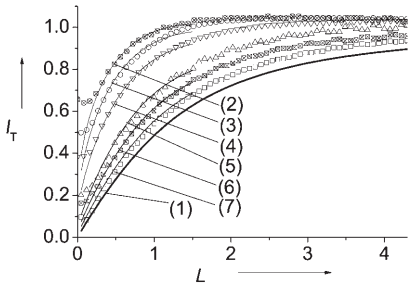

Figure 4. Normalized SECM feedback approach curves for the approach of a Pt disk electrode, $r_T = 13.65\,\mu m$ (curves 2, 3, 4, 6), and $r_T = 12.49\,\mu m$ (curves 5, 7), toward a ZnO/Eosin Y film under illumination by a blue LED. Concentration of I_3^- in mM: 2) 0.033, 3) 0.052, 4) 0.080, 5) 0.495, 6) 0.99, 7) 1.98; scan rate $= 1\,\mu m\,s^{-1}$; $E_T = -0.7$ V; solid lines are calculated curves for the approach of a UME with RG = 10 toward an inert insulating surface[33] (curve 1), and toward samples with first-order kinetics of mediator recycling[12] using normalized rate constants κ: 2) 0.35, 3) 0.27, 4) 0.18, 5) 0.07, 6) 0.04, 7) 0.019.

$$I_T(L) = I_{T,ins}(L) + \left(1-\frac{I_{T,ins}(L)}{I_{T,cond}(L)}\right)I_S(L) \quad (3)$$

This equation considers the contribution $I_{T,ins}(L)$ of hindered diffusion of I_3^- from the bulk solution to the UME and a substrate current $I_S(L)$ that originates from the conversion of the mediator at the sample. $I_{T,cond}(L)$ is the current that results if the reaction at the sample is diffusion-controlled. The degree to which this reaction can influence $I_T(L)$ depends on the normalized distance L and can be calculated as $1-I_{T,ins}/I_{T,cond}$. Analytical approximations for the individual contributions to Equation (3) for $0.1 < L < 1.5$ which were used to form an analytical function to which the individual experimental curves can be fitted are taken from reference [33] [Eqs. (4) and (5)] and reference [12] [Eq. (6)].

$$I_{T,ins}(L) = \frac{1}{0.292 + \frac{1.5151}{L} + 0.6553\exp\left(\frac{-2.4035}{L}\right)} \quad (4)$$

$$I_{T,cond}(L) = 0.68 + \frac{0.78377}{L} + 0.3315\exp\left(\frac{-1.0672}{L}\right) \quad (5)$$

$$I_S(L) = \frac{0.78377}{1 + \frac{1}{\kappa L}} + \frac{0.68 + 0.3315\exp\left(\frac{-1.0672}{L}\right)}{1 + \frac{\frac{11}{\kappa L} + 7.3}{110-40L}},\ 0.1 < L < 1.5 \quad (6)$$

$\kappa = k_{eff}r_T/D$ is a normalized, dimensionless, first-order rate constant which can be obtained by fitting each curve to the analytical approximations. Using the diffusion coefficient of I_3^- in acetonitrile, $D = 1.37\times10^{-5}\,cm^2\,s^{-1}$,[31] and the r_T of the particular UME, the apparent heterogeneous first-order rate constant k_{eff} [$cm\,s^{-1}$] for the reduction of the photo-oxidized dye by I^- can be determined. In Figure 4, curves 2–7 give the experimental variations (open symbols) and the theoretical best fits as thin lines. Deviations at small distances result from a mechanical contact between the insulating sheath of the UME and the sample, after which the distance between the active electrode area and the sample does not decrease further as a result of free translation of the UME in solution (see Experimental Section for more details). The data resulting from the fit are summarized in Table 1. Under the conditions used here, the apparent first-order rate constant k_{eff} decreases with increasing bulk concentration of I_3^-, even at sub-millimolar concentrations.

Table 1. Normalized apparent heterogeneous first-order rate constants κ and apparent heterogeneous first-order rate constants $k_{eff} = \kappa D/r_T$ obtained for the reduction of photoexcited Eosin Y^+ by I^-; $D = 1.37\times10^{-5}\,cm^2\,s^{-1}$.[31]

$[I_3^-]^*$ [$mol\,cm^{-3}$][a]	κ[b]	r_T [μm][c]	k_{eff} [$10^{-3}\,cm\,s^{-1}$]
1.98	0.019	13.65	0.1907
0.99	0.040	13.65	0.4015
0.495	0.070	13.65	0.7026
0.105	0.16	13.65	1.605
0.088	0.18	12.49	1.973
0.052	0.27	13.65	2.710
0.033	0.35	12.49	3.836

[a] Total concentration of I_3^-, I_2, and I^-, given as the equivalent I_3^- concentration in the bulk phase. [b] Dimensionless normalized pseudo-first-order rate constant obtained by fitting experimental approach curves to Equations (3)–(6). [c] Obtained by fitting approach curves to a glass surface.

Relationship of the effective rate constants and microscopic processes in DSSC: To relate k_{eff} to the rate of the microscopic processes in the ZnO/Eosin Y film we consider three major processes in which charges are transported between the UME and the back contact of the ZnO/Eosin Y electrode (Figure 5). By deriving expressions for the limiting current of each individual step, an expression for the normalized substrate current $I_S(L)$ can be found and compared with that of a simple first-order reaction at the sample.

The first step is the reaction at the UME [Eq. (1)]. The limiting current [Eq. (7)] will be measured if the reactions at the UME and at the sample are both diffusion-controlled.

$$i_{T,lim} = i_{T,\infty}I_{T,cond}(L) = 8FD[I_3^-]^*r_TI_{T,cond}(L) \quad (7)$$

The second step is the heterogeneous reaction of I^- with the oxidized dye molecule. To derive kinetic expressions for this situation we need to make some greatly simplifying assumptions about the structure of the ZnO/Eosin Y film. Previous analysis of the film has shown that it is porous and has a total dye loading $\Gamma_{D^\bullet} = 6\times10^{-8}\,mol\,cm^{-2}$ (referred to the geometric area).[9] The film is about 3 μm thick.[9] The dye is homogeneously distributed within the film on a length scale of 500 nm. At present the ratio of the dye molecules that is accessible to I^- under light illumination is unclear. In the model used here, it is assumed that all dye molecules are equally accessible. Furthermore, all Eosin Y molecules have the same excitation cross-section φ_{hv} (that is, the same probability of absorbing a photon entering the film from the

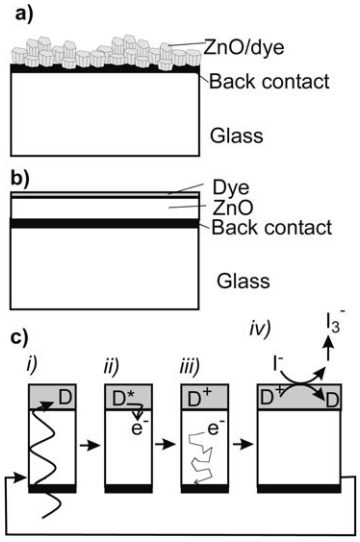

Figure 5. Simplified model of the charge transport between the UME and the ZnO/Eosin Y electrode. The model is not to scale. a) Model of the structure of the nanoparticulate ZnO/Eosin Y film. b) Simplified model in which all dye molecules are uniformly accessible. c) Conceptual sequence of charge transfer processes in the film: i) photoexcitation, ii) electron injection from the dye in the CB of ZnO, iii) electron transport across the ZnO film to the back contact, iv) dye regeneration by reaction with I^-.

back). The neutral dye is denoted by D, photoexcited dye molecules are D*, and photo-oxidized dyes are D^+. Equation (8) gives the kinetically limited current for the process in Equation (2) ($n = 1$, number of transferred electrons; F, Faraday constant; A, geometric area of the sample where I^- is converted, k_{ox} [$cm^{9/2} mol^{-3/2} s^{-1}$], heterogeneous rate constant of order 1.5; Γ_{D+}, steady-state surface concentration of photo-oxidized dye molecules; $[I^-]_S$, concentration of dissolved I^- at the surface of the ZnO film).

$$i_K = nFAk_{ox}\Gamma_{D^+}[I^-]_S{}^{3/2} - i_{rec} \quad (8)$$

The recombination current i_{rec} summarizes the current originating from the reaction of electrons from the conducting glass, from the conduction band of ZnO, and from surface states with I_3^-. For the following analysis this contribution was not considered any further. This greatly simplifying assumption is, however, supported by the following facts: in our setup the Eosin Y-modified ZnO electrode is operated under short-circuit conditions (Figure 2). At the excitation wavelength of 473 nm (see Supporting information), such electrodes have an incident photon–current conversion efficiency (IPCE) of about 80% (see Figure 1 of reference [9]). This means that in short-circuit conditions there is almost no loss by recombination processes. Furthermore, the difference between the IPCE value and 100% also includes contributions from reflection and scattering of light. Close to short-circuit conditions, photocurrent transients do not exhibit an overshoot indicative of recombination. This situation changes if the DSSC is operated under open-circuit conditions. This conclusion is also supported by a recent analysis by Peter et al.,[34] who investigated the contribution of the different recombination pathways at DSSCs made from TiO_2 with and without an additional blocking layer. The blocking layer covers the empty areas on the conducting glass that are left when a TiO_2 particle suspension is applied to the conducting glass. Recombination at the conducting glass was found to be the main recombination pathway under low light intensities such as in our experiments. However, due to the electrochemical nature of the deposition procedure for Eosin Y-modified ZnO, such electrodes have a much smaller fraction of exposed, bare, conducting glass, since the deposition procedure proceeds preferentially on the uncovered regions. Therefore the usual main recombination pathway is not available in our samples.

An expression for Γ_{D+} can be derived from the mass conservation of the dye and the steady-state approximations for surface concentrations of the photoexcited dye Γ_{D^*} [Eqs. (9) and (10)] and the photo-oxidized dye Γ_{D+} [Eqs. (11) and (12)]. Here k_{inj} [s^{-1}] is the first-order rate constant for injection of electrons from the excited dye into the conduction band; $J_{h\nu}$ [$mol\,cm^{-2}s^{-1}$] is the photon flux; Γ_D is the surface concentration of the dye in the ground state.

$$\frac{\partial\Gamma_{D^+}}{dt} = 0 = -k_{ox}\Gamma_{D^+}[I^-]_S{}^{3/2} + k_{inj}\Gamma_{D*} \quad (9)$$

$$\frac{\Gamma_{D^+}}{\Gamma_{D*}} = \frac{k_{inj}}{k_{ox}[I^-]_S{}^{3/2}} \quad (10)$$

$$\frac{\partial\Gamma_{D^*}}{dt} = 0 = \phi_{h\nu}J_{h\nu}\Gamma_D - k_{inj}\Gamma_{D*} \quad (11)$$

$$\frac{\Gamma_D}{\Gamma_{D*}} = \frac{k_{inj}}{\phi_{h\nu}J_{h\nu}} \quad (12)$$

Appropriate substitutions of Eqs. (10) and (12) into the mass conservation law [Eq. (13)] yield an expression for Γ_{D^*}, from which Eq. (14) for Γ_{D+} is obtained by applying Equation (8).

$$\begin{aligned}\Gamma_{D\circ} &= \Gamma_D + \Gamma_{D^+} + \Gamma_{D*} \\ &= \frac{\Gamma_D}{\Gamma_{D*}}\Gamma_{D*^+} + \frac{\Gamma_{D^+}}{\Gamma_{D*}}\Gamma_{D*} + \Gamma_{D*} \\ &= \Gamma_{D*}\left(\frac{k_{inj}}{k_{ox}[I^-]_S{}^{3/2}} + \frac{k_{inj}}{\phi_{h\nu}J_{h\nu}} + 1\right)\end{aligned} \quad (13)$$

$$\Gamma_{D^+} = \frac{k_{inj}}{k_{ox}[I^-]_S{}^{3/2}}\Gamma_{D*} = \Gamma_{D\circ}\frac{1}{1 + \frac{k_{ox}[I^-]_S{}^{3/2}}{\phi_{h\nu}J_{h\nu}} + \frac{k_{ox}[I^-]_S{}^{3/2}}{k_{inj}}} \quad (14)$$

Substituting Equation (14) into Equation (8), and considering that the limiting substrate current $i_{K,lim}$ is obtained if $[I^-]_S$ equals three times the bulk concentration of triiodide $[I_3^-]^*$, leads to Equation (15).

$$i_{K,\mathrm{lim}} = FA\Gamma_{\mathrm{D}\circ}\frac{1}{\frac{1}{k_{\mathrm{ox}}(3[\mathrm{I}^-]^*)^{3/2}} + \frac{1}{\phi_{h\nu}J_{h\nu}} + \frac{1}{k_{\mathrm{inj}}}} \quad (15)$$

Provided that the current distribution is uniform in the sample region directly below the microdisk electrode of the probe, the reciprocal of the normalized substrate current is obtained as the sum of the reciprocal limiting currents of all the consecutive processes: diffusion in the UME–sample gap, passage of kinetically controlled substrate current, and electron conduction to the back contact.[12,35] The limiting kinetic substrate current is again a sequence of heterogeneous electron transfer between I^- and D^+, light absorption by D, and electron injection into the conduction band. By approximating the area of the sample that participates in the electron transfer to πr_T^2, Equation (16) is obtained.

$$\begin{aligned}\frac{1}{I_S} = \frac{i_{T,\infty}}{i_S} &= \frac{1}{I_{T,\mathrm{cond}}} + \frac{4\times 2FDr_T[\mathrm{I_3}^-]^*}{i_K} + \frac{1}{I_{\mathrm{el,lim}}} \\ &= \frac{1}{I_{T,\mathrm{cond}}} + \frac{4}{\pi}\frac{2D[\mathrm{I_3}^-]^*}{r_T\Gamma_{\mathrm{D}\circ}k_{\mathrm{ox}}(3[\mathrm{I_3}^-]^*)^{3/2}} + \frac{4}{\pi}\frac{2D[\mathrm{I_3}^-]^*}{r_T\Gamma_{\mathrm{D}\circ}\phi_{h\nu}J_{h\nu}} \\ &\quad + \frac{4}{\pi}\frac{2D[\mathrm{I_3}^-]^*}{r_T\Gamma_{\mathrm{D}\circ}k_{\mathrm{inj}}} + \frac{1}{I_{\mathrm{el,lim}}}\end{aligned} \quad (16)$$

$I_{\mathrm{el,lim}}$ is the limiting electronic current through the substrate at a given working distance L from the UME. Extensive literature has been devoted to the characterization of this parameter. Recent reports describe the process as diffusion of electrons in the semiconductor rather than voltage-driven electron transport. Diffusion coefficients are comparable with those of solvated ions in the solution. The analysis is complicated by a dependence of the conductivity on the charge carrier density and the electronic structure of the particular ZnO/dye preparation. As the film thickness ($l \leq 3\,\mu m$) is less than the SECM working distance, the electronic conductivity of the film should not become rate-limiting under our experimental conditions if the mobility of the charge carriers is comparable with that of the mediator in solution. We also work with very low electrolyte concentrations compared with conventional DSSC. It should be kept in mind, however, that the present series of experiments were designed purposefully to fulfil the conditions necessary to analyze the interfacial kinetics of dye regeneration. Under DSSC operating conditions this is typically not achieved and conduction in the semiconductor matrix plays a decisive role. Ignoring further a possible back-reaction of conduction band electrons with I_3^- or intermediate I_2 species, we may assume as a first, very coarse, approximation that $1/I_{\mathrm{el,lim}}$ approaches zero in our experiments.

In this case a comparison of Equation (17) (that is, Equation (9) of reference [12]) with Equation (16) and the substitution of $\kappa = k_{\mathrm{eff}}r_T/D$ leads to an approximate expression for the apparent first-order rate constants k_{eff} (see Equation (18) and Table 1); k_{eff} replaces the true first-order rate constant for an uncomplicated electron transfer k_{ET} in Equation (17).

$$\frac{1}{I_S} = \frac{1}{I_{T,\mathrm{cond}}} + \frac{1}{I_{\mathrm{ET}}} = \frac{1}{I_{T,\mathrm{cond}}} + \frac{4}{\pi}\frac{D}{r_Tk_{\mathrm{ET}}} = \frac{1}{I_{T,\mathrm{cond}}} + \frac{4}{\pi}\frac{1}{\kappa} \quad (17)$$

$$\frac{1}{k_{\mathrm{eff}}} = \frac{2}{3\sqrt{3}\Gamma_{\mathrm{D}\circ}k_{\mathrm{ox}}\sqrt{[\mathrm{I_3}^-]^*}} + \frac{2[\mathrm{I_3}^-]^*}{\Gamma_{\mathrm{D}\circ}\phi_{h\nu}J_{h\nu}} + \frac{2[\mathrm{I_3}^-]^*}{\Gamma\Gamma_{\mathrm{D}\circ}k_{\mathrm{inj}}} \quad (18)$$

The apparent first-order rate constant decreases with increasing $[I_3^-]^*$. When $[I_3^-]^*$ increases, the flux of UME-generated I^- will be greater and pseudo-first-order conditions are not maintained at the ZnO/Eosin Y film even at submillimolar triiodide concentrations. This indicates that under the experimental conditions the steady-state concentration of *accessible* photoexcited dye cation Eosin Y^+ in the ZnO film is *not* much greater than the dissolved electron donor concentration and true first-order conditions are not maintained.

Values for k_{ox} [$\mathrm{cm^{9/2}mol^{-3/2}s^{-1}}$] and $1/k_{h\nu,\mathrm{eff}}$ [s] were extracted from the graph of the experimental values $1/k_{\mathrm{eff}}$ [$\mathrm{s\,cm^{-1}}$] versus $[I_3^-]^*$ [$\mathrm{mol\,cm^{-3}}$] in Figure 6 and from Equation (18), using different numerical models (Table 2; for further details see Supporting information). The effective rate constant for the excitation and electron injection process for a given light intensity, wavelength, and dye molecule (contained in $\varphi_{h\nu} = \varphi_{h\nu}(\lambda)$) can be defined as in Equation (19).

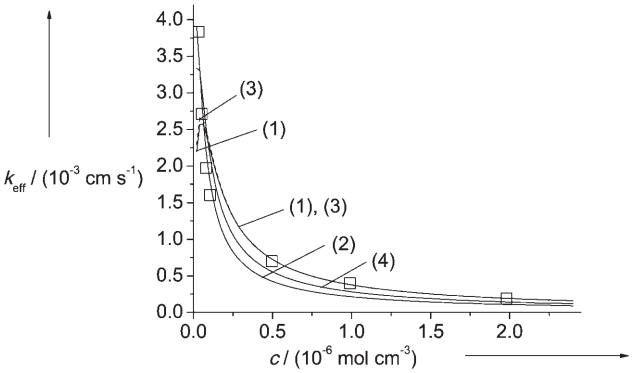

Figure 6. Variation of experimental values of k_{eff} versus bulk concentration of I_3^-. The lines represent different fits of parameters to the data.

$$(k_{h\nu,\mathrm{eff}})^{-1} = (k_{\mathrm{inj}})^{-1} + (\phi_{h\nu}J_{h\nu})^{-1} \quad (19)$$

The values for k_{ox} and $k_{h\nu,\mathrm{eff}}$ were calculated from p_1 and p_2 using experimental total dye loading $\Gamma_{\mathrm{D}\circ} = 6\times 10^{-8}\,\mathrm{mol\,cm^{-2}}$. The uncertainty estimates in Table 2 are the statistical uncertainties of the fitting procedures. Taking into account the uncertainty in the determination of individual κ values, the uncertainty of the values can be expected to be significantly greater than given in Table 2. The different fitting procedures lead to better approximations in different concentration regimes. Summarizing the results in Table 2, a sensible estimate could be $k_{\mathrm{ox}} = (1.4\pm0.8)\times10^8\,\mathrm{cm^{9/2}mol^{-3/2}\,s^{-1}}$, and $1/k_{h\nu,\mathrm{eff}} = (105\pm35)$ s. Since the fluorescence of

Table 2. Numerical models and fitting results for the curves in Figure 6.

	Model[a]	p_1	p_2	k_{ox} [10^8 cm$^{9/2}$mol$^{-3/2}$s^{-1}][b]	$1/k_{hv,eff}$ [s][b]
1	$\frac{1}{k_{eff}} = p_1\frac{1}{\sqrt{c}+p_2 c}$	$p_1 = \frac{2}{3\sqrt{3}\Gamma_{D^\bullet}k_{ox}}$	$p_2 = \frac{2}{\Gamma_{D^\bullet}k_{hv,eff}}$	1.12 (±23%)	78.1 (±2%)
2	$k_{eff} = \frac{p_1\sqrt{c}}{p_2+2c}$	$p_1 = \Gamma_{D^\bullet}k_{hv,eff}$	$p_2 = \frac{2k_{hv,eff}}{3\sqrt{3}k_{ox}}$	2.78 (±23%)	140 (±6%)
3	$\frac{\sqrt{c}}{k_{eff}} = p_1 + p_2 c^{3/2}$	$p_1 = \frac{2}{3\sqrt{3}\Gamma_{D^\bullet}k_{ox}}$	$p_2 = \frac{2}{\Gamma_{D^\bullet}k_{hv,eff}}$	1.18 (±80%)	78.4 (±1%)
4	$\frac{1}{ck_{eff}} = p_1\frac{1}{c^{3/2}} + p_2$	$p_1 = \frac{2}{3\sqrt{3}\Gamma_{D^\bullet}k_{ox}}$	$p_2 = \frac{2}{\Gamma_{D^\bullet}k_{hv,eff}}$	1.98 (±36%)	106 (±17%)

[a] The symbol c stands for $[I_3^-]$*. [b] The values for k_{ox} and $k_{hv,eff}$ were calculated from p_1 and p_2 using $\Gamma_{D^\bullet} = 6\times10^{-8}$ mol cm^{-2}.

Eosin Y is completely quenched when the dye is adsorbed onto ZnO, it is reasonable to assume that k_{inj} is in the same order as for a fluorescence process and, therefore, $(k_{hv,eff})^{-1} \approx (\varphi_{hv}J_{hv})^{-1}$. Taking the measured photon flux to be 3.9×10^{-9} mol s^{-1} cm^{-2}, the photoexcitation cross-section of the adsorbed dye molecule can be estimated as 2.4×10^6 cm^{2}mol^{-1} or 4×10^{-2} Å^2 per individual dye molecule. As expected, this cross-section is much smaller than the geometrical cross-section of an adsorbed dye molecule.

The physical interpretation of these numbers should be carried out with caution, keeping in mind the assumptions used in deriving them. In particular, it is currently unclear which fraction of the dye molecules takes part in the photoexcitation and regeneration process and how this number is influenced by the structural parameters of the nanoparticulate ZnO/Eosin Y film. While it seems reasonable that not all the adsorbed dye molecules are accessible to dissolved I^-, inaccessible dye molecules may nevertheless contribute notably to a photocurrent if they are provided with electrons by a fast lateral charge transfer along a layer of adsorbed (and probably aligned) dye molecules. Consequently, the quantities derived above are representative values for an ensemble that characterize a particular preparation of a ZnO/Eosin Y DSSC, while the true molecular equivalents of these quantities have a very broad dispersion.

SECM was applied to investigate the electrode reactions of dye-sensitized solar cells (DSSC) for the first time. Electrodes based on nanocrystalline ZnO/Eosin Y films were chosen as an example. The mediator concentration used in this study was much lower than that in practical DSSC applications. It was found experimentally that even at sub-millimolar triiodide concentrations the observed normalized rate constant from SECM approach curves depended on the concentration. A detailed kinetic analysis made it possible to relate the observed approach curves to a kinetic model of the dye regeneration process under the short-circuit operation conditions of the DSSC and low light intensities. Effective rate constants could be determined for the dye regeneration by electron transfer from the electrolyte ($(1.4\pm0.8)\times10^8$ cm$^{9/2}$mol$^{-3/2}$s^{-1}) and were related to the rates of photoexcitation and electron injection for a given experimental setup. The analysis showed further that only a minute fraction of the total dye load participated in the reaction with the dissolved donor. Despite the greatly simplifying assumptions made during the data analysis, the method is opening the way for further studies to elucidate the relationships between the structural characteristics of the dye-sensitized semiconductors and the characteristic properties accessible by SECM experiments. Extension of the applicability to other material combinations of DSSCs and other electrolyte systems seems straightforward. In the future such measurements can complement existing DSSC characterization methods from both physico-chemical and engineering points of view.

Experimental Section

Chemicals: Acetonitrile (Spectrochem, HPLC grade), the solvent for the electrolyte solution, was purified as described in reference [32]. Anhydrous tetrabutylammonium trifluoromethanesulfonate (TBAS) (electrochemical grade, Fluka) was used as supporting electrolyte without further purification. I_2 (Merck) was purified by sublimation before use. KI was pretreated by heating at 150 °C for 3 h and then dried in vacuum before use. Solutions of KI_3 in acetonitrile/TBAS were prepared by mixing equimolar portions of 4 mM solutions of KI and I_2 in acetonitrile/TBAS and diluting the resulting stock solution to the required concentration with acetonitrile/TBAS electrolyte solution.

Preparation of ZnO/Eosin Y film samples: The ZnO/Eosin Y hybrid thin films used as samples were prepared in a three-electrode single-compartment cell with a saturated calomel electrode (SCE) as reference electrode, a Zn wire as counter-electrode and F-doped SnO_2 on glass (Asahi Glass) as working electrode.[9,36] The F-doped SnO_2 glass substrate was mounted as a rotating electrode in a stainless steel holder providing mechanical and electrical attachment to a rotating disk electrode (RDE) system and was operated at 500 rpm. The ZnO/Eosin Y films were deposited at −1.0 V (vs. SCE) for 20 min at 70 °C from an oxygen-saturated aqueous solution containing 5 mM $ZnCl_2$ (Fluka), 0.1 M KCl (Roth), and 50 μM Eosin Y (Aldrich). The solution was purged with O_2 at a volume flow rate of 200 mL min^{-1}. Following deposition, the ZnO/Eosin Y film was exposed to a dilute aqueous KOH solution (pH 10.5) for 24 h to desorb the loaded Eosin Y molecules. The films were dried in air for 1 h at 150 °C. Eosin Y was re-adsorbed from aqueous 250 μM Eosin Y solutions at 80 °C.

Instruments and procedures: SECM experiments were performed on a home-built instrument.[37] The Teflon cell contained a Pt wire counter-electrode and a Pt wire quasi-reference electrode. The ZnO/Eosin Y sample film was attached to the bottom of the cell and sealed by an O-ring. An extra Pt wire connected the back contact of the ZnO/Eosin Y sample with the electrolyte to operate the photoelectrochemical cell in a short-circuit setup. All potentials are given with respect to the quasi-reference electrode used in the particular experiment. This reference value may have varied slightly, depending on solution composition. Positioning was performed with an x–y–z stepper motor system (Scientific Precision Instruments, Oppenheim, Germany). For all the SECM experiments, a monopotentiostat μ-P3 (M. Schramm, Heinrich Heine University, Düsseldorf, Germany) was used. Data were processed and analyzed with the in-house software MIRA.

A Pt wire (Goodfellow, Cambridge, UK), diameter 25 μm, was sealed into a 5 cm Pyrex glass capillary under vacuum. The UME was polished and shaped conically by a wheel with 180-grid Carbimet paper disks and micropolishing cloths with 1.0 μm, 0.3 μm, and 0.05 μm alumina. The UME was sharpened to RG ~ 10, where RG is the ratio of the diameters of the glass sheath and the Pt wire. Before each experiment, the UME was polished with 0.3 and 0.05 μm alumina powder and rinsed with water. After the UME had been mounted, an approach curve was recorded toward a smooth glass surface until the mechanical contact between

the glass sheath of the UME and the sample surface was detected by a suddenly established constant current (for example, at $L = 0.25$ in Figure 3). By a fit to the well-established theoretical curve for this situation [Eq. (4)], the exact r_T and the distance d_0 between the *active* electrode surface and the sample at the moment of mechanical contact by the insulating sheaths were detected. This distance d_0 was determined by the shape of the UME, the exact mounting geometry, and the tilt of the sample. The UME was completely retracted afterward, but the mounting was not changed. The glass sample was exchanged for the Eosin Y/ZnO sample, then approach curves to the Eosin Y/ZnO samples under illumination were recorded. By fitting the data to theoretical curves [Eqs. (3)–(5)], it was assumed that d_0 was the same as d_0 determined for the glass sample, because the UME geometry and the sample tilt were identical in the two situations. The point of closest approach could be identified clearly by the sudden deviation from the expected behavior for the approach curves. When r_T and the coordinates of the surface in the positioning system were known, the curves could be fitted to the theoretical curves by adjusting κ and $i_{T,\infty}$. We found this procedure to be necessary in order to separate the different unknown variables clearly.

All the experiments were carried out at room temperature. Illumination from a blue light-emitting diode (LED, 2000 MCD Blue; Reichelt Elektronik, Sande, Germany) was focused onto the back of the ZnO/Eosin Y film. The photon flux was 3.9×10^{-9} mol s^{-1} cm^{-2} measured by a calibrated photodiode (Hamamatsu). The excitation light did not contain contributions below 420 nm that could lead to direct photoexcitation of ZnO (band gap 3.2 eV corresponding to 386 nm; see Supporting information).

Acknowledgements

The help of Prof. Dr. Wilfried Tuszynski and Dirk Otteken (Institut für Physik, Universität Oldenburg) in the measurement of the photon flux is gratefully acknowledged. Constructive comments of two anonymous referees considerably improved the quality of the manuscript. Part of this work was supported by the Volkswagen Foundation under grant number I/80314. Y.S. thanks the Hanse Institute of Advanced Studies Delmenhorst and the Alexander von Humboldt Foundation for research fellowships.

[1] B. O'Regan, M. Grätzel, *Nature* **1991**, *353*, 737–740.
[2] S. Lindquist, A. Hagfeldt, S. Södergren, H. Lindström, Charge transport in nanostructured thin-film electrodes, in *Electrochemistry of Nanomaterials* (Ed.: G. Hodes), Wiley-VCH, Weinheim, **2001**, Ch. 6.
[3] J. Nelson, in *Encyclopedia of Electrochemistry, Vol. 6* (Eds.: A. J. Bard, M. Stratmann, S. Licht), Wiley-VCH, Weinheim, **2002**, pp. 432–474.
[4] K. Hara, K, Sayama, Y. Ohga, A. Shinpo, S. Sugar, H. Arakawa, *Chem. Commun.* **2001**, 569–570.
[5] M. K. Nazeeruddin, M. Grätzel, in *Encyclopedia of Electrochemistry, Vol. 6* (Eds.: A. J. Bard, M. Stratmann, S. Licht) Wiley-VCH, Weinheim, **2002**, pp. 407–431.
[6] E. Palomares, J. N. Clifford, S. A. Haque, T. Lutz, J. R. Durrant, *J. Am. Chem. Soc.* **2003**, *125*, 475–482.
[7] A. C. Fisher, L. M. Peter, E. A. Ponomarev, A. B. Walker, K. G. U. Wijayantha, *J. Phys. Chem. B* **2000**, *104*, 949–958.
[8] T. Yoshida, T. Oekermann, K. Okabe, D. Schlettwein, K. Funabiki, H. Minoura, *Electrochemistry* **2002**, *70*, 470–487.
[9] T. Yoshida, M. Iwaya, H. Ando, T. Oekermann, K. Nonomura, D. Schlettwein, D. Wöhrle, H. Minoura, *Chem. Commun.* **2004**, 400–401.
[10] N. S. Lewis, *J. Phys. Chem. B* **1998**, *102*, 4843–4855.
[11] C. Combellas, J. Ghilane, F. Kanoufi, D. Mazouzi, *J. Phys. Chem. B* **2004**, *108*, 6391–6397.
[12] C. Wei, A. J. Bard, M. V. Mirkin, *J. Phys. Chem.* **1995**, *99*, 16033–16042.
[13] Y. Selzer, D. Mandler, *J. Electroanal. Chem.* **1996**, *409*, 15–17.
[14] C. J. Slevin, J. V. Macpherson, P. R. Unwin, *J. Phys. Chem. B* **1997**, *101*, 10851–10859.
[15] M. V. Mirkin, M. Tsionsky, in *Scanning Electrochemical Microscopy* (Eds.: A. J. Bard, M. V. Mirkin), M. Dekker, New York, **2001**, pp. 299–342.
[16] D. T. Pierce, P. R. Unwin, A. J. Bard, *Anal. Chem.* **1992**, *64*, 1795–1804.
[17] C. Zhao, G. Wittstock, *Anal. Chem.* **2004**, *76*, 3145–3154.
[18] C. Zhao, J. Sinha, C. A. Wijayawardhana, G. Wittstock, *J. Electroanal. Chem.* **2004**, *561*, 83–91.
[19] S. B. Basame, H. S. White, *J. Phys. Chem.* **1995**, *99*, 16430–16435.
[20] P. James, N. Casillas, W. H. Smyrl, *J. Electrochem. Soc.* **1996**, *143*, 3853.
[21] S. B. Basame, H. S. White, *Langmuir* **1999**, *15*, 819–825.
[22] S. B. Basame, H. S. White, *Anal. Chem.* **1999**, *71*, 3166–3170.
[23] I. Serebrennikova, S. Lee, H. S. White, *Faraday Discuss.* **2002**, *121*, 199–210.
[24] D. Mandler, A. J. Bard, *Langmuir* **1990**, *6*, 1489–1494.
[25] B. R. Horrocks, M. V. Mirkin, A. J. Bard, *J. Phys. Chem.* **1994**, *98*, 9106–9114.
[26] H. Maeda, K. Ikeda, K. Hashimoto, K. Ajito, M. Morita, A. Fujishima, *J. Phys. Chem. B* **1999**, *103*, 3213–3217.
[27] S. M. Fonseca, A. L. Barker, S. Ahmend, T. J. Kemp, P. R. Unwin, *Chem. Commun.* **2003**, 1002–1003.
[28] T. J. Kemp, P. R. Unwin, L. Vincze, *J. Chem. Soc. Faraday Trans.* **1995**, *91*, 3893–3896.
[29] S. K. Haram, A. J. Bard, *J. Phys. Chem. B* **2001**, *105*, 8192–8195.
[30] B. Liu, A. J. Bard, M. V. Mirkin, *J. Am. Chem. Soc.* **2004**, *126*, 1485–1492.
[31] V. A. Macagno, M. C. Giordano, A. J. Arvia, *Electrochim. Acta* **1969**, *14*, 335–357.
[32] G. Rothenberger, D. Fitzmaurice, M. Grätzel, *J. Phys. Chem.* **1992**, *96*, 5983–5986.
[33] J. L. Amphlett, G. Denuault, *J. Phys. Chem. B* **1998**, *102*, 9946–9951.
[34] P. J Cameron, L. M. Peter, S. Hore, *J. Phys. Chem. B* **2005**, *109*, 930–936.
[35] C. P. Andrieux, J. M. Savéant, *J. Electroanal. Chem.* **1982**, *134*, 163–166.
[36] T. Yoshida, D. Komatsu, N. Shimokawa, H. Minoura, *Thin Solid Films* **2004**, *451–452*, 166–169.
[37] T. Wilhelm, G. Wittstock, *Langmuir* **2002**, *18*, 9485–9493.

Received: October 8, 2005
Revised: February 9, 2006
Published online: May 9, 2006

